Type 3 ryanodine receptors of skeletal muscle are segregated in a parajunctional position

Edward Felder* and Clara Franzini-Armstrong

Department of Cell and Developmental Biology, University of Pennsylvania, Philadelphia, PA 19104-6058

Contributed by Clara Franzini-Armstrong, December 10, 2001

A key event in skeletal muscle activation is the rapid release of Ca^{2+} from the sarcoplasmic reticulum (SR), the Ca^{2+} storage organelle in the muscle cell. The surface membrane/transverse tubules and the SR form functional units (calcium release units containing one or two couplons or junctions), where the voltage-sensing dihydropyridine receptor of the surface membrane interacts with the SR Ca^{2+} release channel [ryanodine receptor (RyR)] and depolarization of the cell membrane is converted into Ca^{2+} release from the SR. Although RyR1 is the most important isoform in skeletal muscle, some muscles also express high levels of RyR3, an isoform with a wide tissue distribution. The cytoplasmic domains of RyRs are visible in the electron microscope as periodically disposed feet. We find that, in muscles containing only RyR1, feet are exclusively located over the junctional SR surface facing the surface membrane/transverse tubule. In muscles containing RyR1 as well as RyR3, additional feet are located in lateral parajunctional regions immediately adjacent to junctional SR. Biochemical content of RyR3 and content of parajunctional feet are highly correlated in different muscles and the disposition of parajunctional versus junctional feet are notably different. On the basis of these two observations, we postulate that RyR3s are restricted to the parajunctional region, and thus their activation must be indirect and derivative during excitation–contraction coupling.

Contraction of muscle myofibrils is activated by Ca^{2+} released from the sarcoplasmic reticulum (SR), a specialized Ca^{2+} sequestering organelle. The trigger for Ca^{2+} release is depolarization of the cell membrane, which is detected by the voltage sensing dihydropyridine receptor (DHPR), a Ca^{2+} channel located in the surface membrane/transverse (T) tubules. In skeletal muscle, the DHPR forms a unique functional and spatial unit with another Ca^{2+} channel: the ryanodine receptor (RyR) or Ca^{2+} release channel of the SR. Voltage-dependent conformational changes of the DHPR are "mechanically" transmitted to the RyR, which responds with Ca^{2+} release (1–3). The whole process, starting with depolarization and resulting in contraction, is called excitation–contraction (e-c) coupling.

Direct interaction between the two Ca^{2+} channels occurs at sites of close apposition or junction between exterior membrane and SR, called calcium release units (CRUs). These junctional complexes are found in the cell interior as SR-T tubule junctions (triads and dyads) in adult skeletal muscle fibers. In CRUs, RyRs are arranged in ordered parallel rows in the junctional SR membrane facing the attached T tubule. RyRs' cytoplasmic domains ("feet") are located in the junctional gap between the SR and T tubule membranes and are clearly visible in the electron microscope (4). The four corners of the tetrafoil-shaped cytoplasmic domain of RyR are each linked to a single DHPR in the apposed T tubule membrane, so that four DHPRs arrange in a characteristic square shape called a tetrad. However, only every other RyR in a row faces a DHPR tetrad in a variety of muscles (refs. 4 and 5; for review, see ref. 6).

There are three known isoforms of the RyR. RyR1 and RyR2 play essential roles in skeletal and cardiac muscle, respectively. The function of RyR3, even though it is very widely distributed in a variety of tissues, is less well understood. Skeletal muscle expresses RyR1 and greatly variable amounts of RyR3 (see refs. 7 and 8 for reviews). These variations are specific for different phyla but can also represent a unique feature of particular species and/or muscles (9). Both isoforms may be present within the same muscle cell and are located in the triads (10–13).

It is clear that RyR1 is the key isoform in terms of skeletal muscle activation as many skeletal muscles, including some very fast ones, express only RyR1, proving that RyR1 alone can sustain effective e-c coupling (9, 13–16). Only RyR1 is capable of forging the link with α1sDHPR necessary for skeletal muscle type e-c coupling and for the organization of four DHPRs into a tetrad (17). RyR3, on the other hand, does not sustain e-c coupling. Muscles developing in the absence of RyR1 as a result of a lethal genetic mutation show strong developmental defects and lack of e-c coupling, despite the presence of RyR3 (18, 19). Even when expressed at high levels, RyR3 alone does not induce restoration of e-c coupling (20) and tetrad formation by DHPRs (17). RyR3 seems to play a minor role in e-c coupling of mouse skeletal muscle, because changes resulting from an engineered RyR 1 null mutation are subtle (16, 21). This effect, however, may be because of the low content of RyR3 in mouse muscle rather than lack of RyR3 function.

We have compared the arrays of feet in triads containing either only RyR1 or different ratios of RyR1 and RyR3. We find that muscles expressing RyR3 have additional feet (parajunctional feet) located in the SR membrane immediately adjacent to, but not within, the junctional region. We suggest that RyR3s are segregated from junctional RyR1 and are either exclusively or mostly located in a parajunctional position. Interestingly, the geometry of the RyR3 array is quite different from that of RyR1.

Materials and Methods

Semitendinosus and sartorius from *Rana pipiens* and *Rana temporaria* (referred to all as frog leg muscles); diaphragm and extensor digitorum longus (EDL) from mouse; swim bladder from toadfish (*Opsanus tau*) and white swim muscle from toadfish and guppy were fixed at room temperature in 3.5–6% glutaraldehyde/0.1 M cacodylate buffer (pH 7.4) and stored at 4°C. The tissue was postfixed in 2% OsO_4/cacodylate buffer, *en bloc* stained with saturated aqueous uranyl acetate at room temperature and embedded in Epon. Sections were stained with uranyl acetate and a solution of lead salts.

For freeze–fracture, the glutaraldehyde fixed tissues were cryoprotected in 30% (vol/vol) glycerol, frozen in liquid propane, fractured, and shadowed in a Balzer's 400 freeze–fracture. Freeze–fractures and sections were examined in a Philips 410 electron microscope.

For counting of feet, images of profiles showing sharp membrane views were collected for each muscle. For measurements of intertetrad distances, T tubule views showing long segments (4 tetrads or more) were selected. Micrographs of toadfish swim

Abbreviations: SR, sarcoplasmic reticulum; DHPR, dihydropyridine receptor; T, transverse; RyR, ryanodine receptor; e-c, excitation–contraction; EDL, extensor digitorum longus.

*To whom reprint requests should be addressed. E-mail: edfelder@mail.med.upenn.edu.

The publication costs of this article were defrayed in part by page charge payment. This article must therefore be hereby marked "*advertisement*" in accordance with 18 U.S.C. §1734 solely to indicate this fact.

PHYSIOLOGY

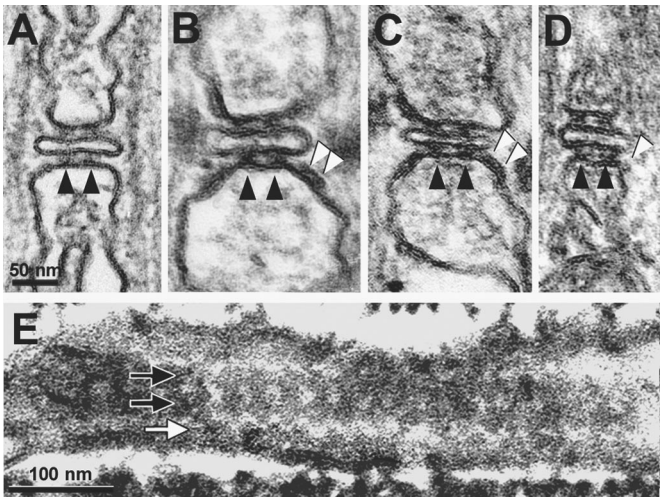

Fig. 1. Views of triads from: (*A*) toadfish swim bladder (expressing no RyR3); (*B*) toadfish white swim muscle (≈50% RyR3); (*C*) *Rana pipiens semitendinosus* (≈50% RyR3); (*D*) mouse diaphragm at day 10 after birth (low level of RyR3). Junctional (black arrowheads) and parajunctional (white arrowheads) feet are indicated. *E* shows a tangent view of the junction in the swim muscle of a small fish (guppy). Two rows of junctional feet (black-on-white arrows) illustrate the tetrafoil shape of single feet and the orthogonal (ladder like) arrangement of junctional feet. A row of parajunctional feet (white on black arrow) shows displacement of parajunctional feet array by half a period relative to the junctional rows. A protein free (white) zigzag strip separates junctional and parajunctional feet.

bladder and guppy swim muscles were part of a previous collection (4, 5). Measurements were performed on digitized images by using NIH IMAGE software.

Results

Junctional and Parajunctional Feet. Fig. 1*A* shows a triad in the toadfish swim-bladder muscle, which contains only RyR1 (9). Two electron dense feet, or RyRs (black arrowheads), occupy the junctional gap on either side of the T tubule. The two feet are part of two long rows running parallel to the T tubule axis, which is perpendicular to the section plane. Parajunctional areas in this muscle show no feet. Fig. 1 *B* and *C* show triads from toadfish white swim muscle and frog sartorius. These muscles and/or their homologues in related species have an ≈50% content of RyR3 (9, 22, 23). In addition to the two sets of junctional feet (black arrowheads), these triads show large elongated densities over the parajunctional SR on either side of the junction (white arrowheads). In some views, the elongated densities resolve themselves into two separate structures (feet, arrowheads, Fig. 1*B*). A small gap separates the junctional feet from the parajunctional densities.

Mammalian skeletal muscles have a fairly low and variable content of RyR3 (10, 13, 24). The content is higher in younger muscles, especially in the diaphragm (10, 16, 25). Parajunctional densities are present in muscles from young mice (Fig. 1*D*; white arrowhead), but they are less frequent and smaller than in frog leg and fish swim muscles.

Figs. 1*E* shows a section parallel to the T tubule axis and grazing the junctional gap in the swim muscle from a small fish, the guppy. Swim muscles in fish have two types of RyRs (9). Along the center of the image are two clearly visible rows of junctional feet (black arrows), identified by their quadrefoil structure and the highly ordered, tetragonal arrangement, resembling a "ladder" in which each "step" is confined by two feet (RyRs). Below the two junctional rows is an additional parallel row of quadrefoils or feet (white arrow). This row is close to, but separate from, the two junctional rows, and its position corresponds to the parajunctional densities shown in Fig. 1 *B–D*. Junctional and parajunctional feet have same spacings within one row, but the entire row of the latter are displaced by a half period. Only one row of parajunctional feet is visible in Fig. 1*E*, but the cross-sectional images (Fig. 1 *B* and *C*) imply that a double row should be present. The second row is not visible in this view, because either the SR membrane becomes perpendicular to the plane of the section at larger distances from the junction or it is not included in the section thickness.

Note the discontinuity between the rows of junctional and parajunctional feet: a clear jagged band separates them. The outlines of feet are closely apposed, almost touching each other within the same row, but there is apparently no contact between the feet in junctional and parajunctional regions (Fig. 1 *B* and *C*).

Junctional and Parajunctional Pits and Bumps in Freeze–Fracture. The channel domains of RyRs span the SR membrane and are split within the lipid bilayer in the process of freeze–fracture. Their profiles are best visible in the luminal leaflet of the SR, where a small pit surrounded by a barely raised platform (bump) marks the position of each foot (4, 5). Fig. 2*A* shows a freeze–fracture of junctional SR in a triad from the toadfish swim-bladder muscle, containing only RyR1. The luminal leaflet of the SR exhibits a double row of pits and bumps (black arrowheads) in the junctional region. The pits define a ladder-like disposition identical to that of junctional feet, as presented in Fig. 1*E*. In muscles with a high level of RyR3 (Fig. 2 *B* and *C*), in addition to the two rows of junctional pits (black arrows), there are additional rows of parajunctional pits (white arrows). Fig. 2 *D* and *E* are duplicates of Fig. 2 *B* and *C*, in which the positions of parajunctional pits are indicated by white-on-black dots and that of junctional pits by black dots. Note that the two sets of pits have distinctly different dispositions. Junctional pits are tetragonally arranged, that is the pits in the two rows are in register. The parajunctional pits, instead, form a zigzag pattern, because the pits are displaced by a half period. In addition, the parajunctional rows are located in a region of the SR, which curves away from the junctional domain.

The parajunctional location of the additional rows of pits in the RyR3-containing frog leg and fish swim muscles is confirmed by fractures in planes parallel to the long axis of the muscle fiber (Fig. 3 *A* and *C–E*). The fracture plane in Fig. 3 *A* and *C–E* follows the myofibril-facing SR and T tubule surfaces, as indicated in Fig. 3*B*. The luminal leaflet of the parajunctional SR membrane shows two rows of pits running parallel to the long axis of the T tubules (white arrows, Fig. 3 *C–E*). As observed above, these parajunctional pits are disposed in a zigzag pattern (see white arrowheads, Fig. 3 *C–E*) quite different from the tetragonal arrangement of junctional pits.

The presence and frequency of parajunctional rows of bumps/pits seen by freeze–fracture corresponds well with the presence, frequency, and size of the parajunctional densities seen in thin sections. Toadfish swim-bladder muscle (RyR1 only) shows neither parajunctional densities in thin sections nor rows of parajunctional bumps/pits; frog leg and fish swim muscles (RyR3/RyR1≈1:1) frequently show large parajunctional densities and double rows of pits; mouse muscle (RyR1≫RyR3) shows less frequent and small parajunctional densities, corresponding to rare single rows of pits. Even where they are most abundant, the parajunctional rows do not always run continuously along the whole length of each SR cisterna but may be absent from some portions of it.

RyR Spacings. The distance between pits along the longitudinal axis of the junction is the same for junctional and parajunctional feet and in different species. Combined values for frog leg and toadfish swim muscle are 28 ± 4 nm (mean ± 1 SD, $n = 298$),

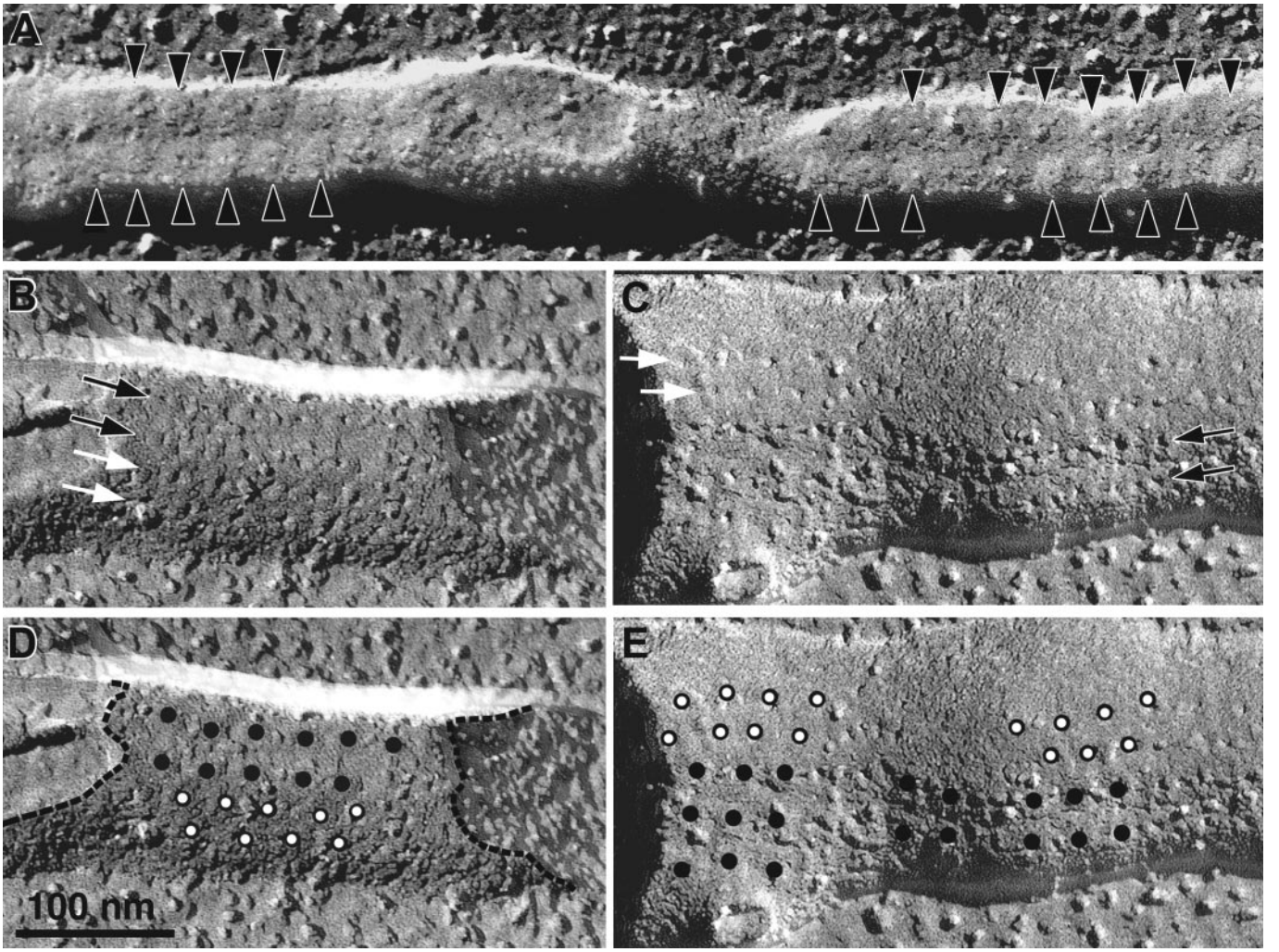

Fig. 2. Luminal leaflets of freeze–fractured SR showing junctional and one of the adjacent parajunctional domains from (*A*) toadfish swim bladder, (*B–E*) *Rana pipiens sartorius*. The fractured intramembrane domains of RyRs appear as small pits surrounded by a shallow bump. Black arrowheads in *A* indicate the positions of individual RyRs; black and white arrows in *B* and *C* indicate the direction of junctional and parajunctional rows of RyRs. *D* and *E* are repeats of *B* and *C*, with the pit positions marked by dots. Junctional RyRs (dots) form an orthogonal (ladder-like) arrangement. Parajunctional RyRs (white-on-black dots) form a zigzag pattern. Note that parajunctional rows are located over membrane domains that curve away from the flat junctional domains (see dashed line following the membrane edge).

in agreement with published data (5). However, the distances between the rows differ in junctional and parajunctional regions. The center to center distances between the rows were measured in triad profiles from thin sections of muscles with a high RyR3/RyR1 ratio (e.g., see Fig. 1 *A–D*). Data from frog leg and toadfish swim muscles are consistent with each other and were combined. The junctional rows are 36 ± 3 nm (n = 36) apart from each other; the distance between the junctional and nearest parajunctional row is 28 ± 7 nm (n = 64) and the distance between the two parajunctional rows is 19 ± 4 nm (n = 39). The accuracy of these measurements is limited by some uncertainty on the exact location of feet centers and also by membrane curvature.

Because the centers of parajunctional feet are the least well precisely located in thin section but are clearly visible in freeze–fracture, we used this technique to confirm the interparajunctional row distance. The interparajunctional row distance measured in freezed–fracture of the same muscles used for thin-section analysis is 17 ± 3 nm (n = 40). This measurement is affected by the variable viewing angle of the membrane. Even if corrected by the effect of a 45° viewing angle (that is by a factor of 1.4), this distance is shorter than the spacing between junctional rows. Overall, measurements from thin sections and freeze–fracture confirm each other, indicating that the inter-row distances are different in the junctional and parajunctional regions emphasizing different disposition of feet.

Relative Content of Junctional and Parajunctional Feet in Muscles with Different RyR3/RyR1 Ratios. The ratio of parajunctional versus junctional feet content was obtained from morphometric analysis of thin sections from two muscles with a high content of RyR3 (frog leg and toadfish swim muscles) and two muscles with a lower RyR3/RyR1 ratio (mouse diaphragm and EDL). In each triad/dyad profile, the number of parajunctional and junctional rows was counted for each couplon (that is for one side of the T tubule; ref. 26). In frog and toadfish, where freeze–fracture shows that each parajunctional profile contains two feet, the profile was counted as two. In mouse, the profile was given the value of either one or (less frequently) two feet, depending on the length of the density, which showed considerable differences in this species. The junctional feet are practically always two in each profile. We calculated the ratio of parajunctional to junc-

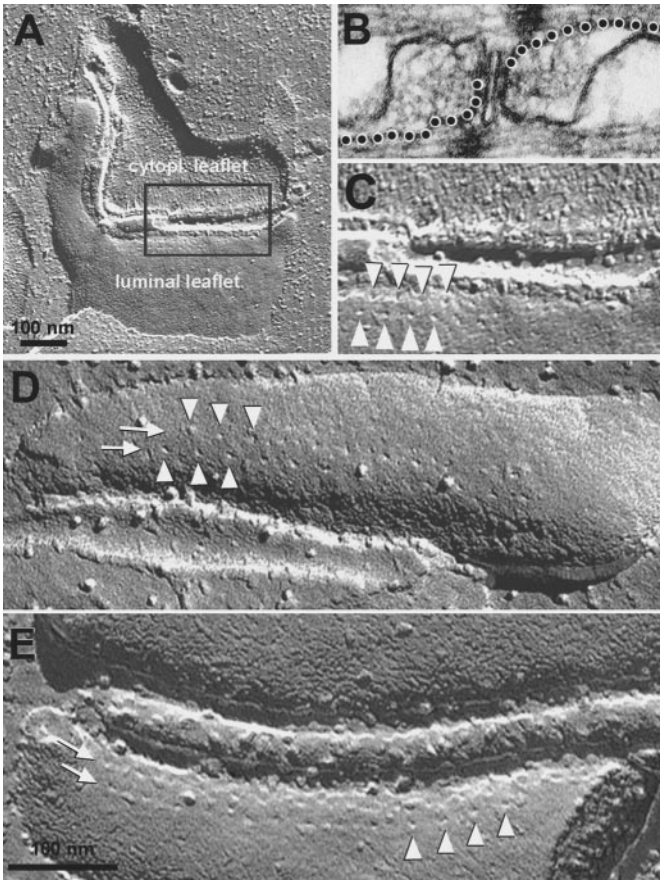

Fig. 3. Freeze–fractures of junctions from muscles with ≈50% RyR3. The plane of fracture is parallel to the fiber long axis, and the triad membranes are split as indicated by the dotted line in *B*, resulting in views of SR parajunctional domains (*A*). (*A*, *C*, *D*) Frog leg muscle; (*E*) toadfish swim muscle. *C–E* show parajunctional pits (white arrowheads), forming two rows (white arrows) with staggered elements in a zigzag pattern.

tional feet for each sectioned couplon profile and the averaged results are given in Table 1. The ratios vary from 1.6 and 1.1 for fish and frog muscles to 0.4 and 0.2 for diaphragm and EDL muscles from young mice and are presented in Table 1.

In the mouse EDL, the RyR3 content varies greatly between individual fibers, whereas in the diaphragm, the content is more uniform (10). For these muscles, we therefore also separately determined the RyR3/RyR1 ratios for individual fibers. The frequency distribution of the parajunctional to junctional feet ratio in single fibers differs between the two muscles (Fig. 4*A*). Fibers from the diaphragm at day 7 show a more homogenous distribution and an overall higher content of parajunctional feet than fibers from EDL at day 10, consistent with (10).

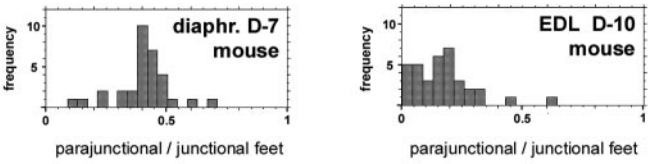

Fig. 4. Frequency histogram showing the ratio of parajunctional/junctional feet for single fibers of mouse diaphragm at day 7 and EDL at day 10. EDL shows smaller and more variable ratios than the diaphragm.

DHPR–Tetrads Spacings. Because RyR1 but not RyR3 is capable of inducing DHPR disposition into tetrads (17), it is interesting to see whether the presence of RyR3 in a given muscle affects the spacing between tetrads. We compared the position of DHPR tetrads in the swim-bladder and the white swim muscle of toadfish that have a RyR3/RyR1 ratio of 0 and ≈1, respectively. Freeze–fractures of both muscles (Fig. 5 *A* and *C*) show two rows of tetrads in the cytoplasmic leaflet of the junctional T tubule membrane. Labeling the center of each tetrad with a dot (Fig. 5 *B* and *D*) helps in visualizing their position, particularly when the tetrads are incomplete, i.e., they lack one or more of the four particles. With very few exceptions (see arrow in Fig. 5*D*), all particles in the fractured T tubule membrane cluster around dots that define two evenly spaced rows and are displaced by a half -period relative to each other. Starting with the tetrad at one end of each row, the distances to all other tetrads along the same row were measured in a number of micrographs, as indicated by the dark bars in Fig. 5 *B* and *D*. To avoid errors caused by variations in the magnification and/or tilt of the image, the measurements for each photograph were standardized against the average distance between tetrads in the same image. The results are plotted in Fig. 5 *E* and *F*. The histograms for the two muscles are identical. Both show regularly spaced peaks at distances that are multiples of the average intertetrad spacing. The absolute value of this distance is 55–60 nm for the both muscles, twice the distance between junctional feet given above, in agreement with previously published results for the toadfish swim bladder (4, 5). Thus tetrads are regularly associated with alternate feet regardless of the presence or absence of RyR3.

A Model of Junctional and Parajunctional Feet Disposition. On the basis of the above observations, the arrangement of junctional and parajunctional feet and of DHPR tetrads in a triad containing a high level of RyR3 is reconstructed in Fig. 6. Two rows of junctional feet (blue profiles) occupy the long axis of the junction. The feet interact with each other close to their corners, and their position is slightly skewed relative to the long axis of the junction (27). Tetrads in the T tubules are associated with alternate junctional feet. Two rows of parajunctional feet (green profiles) are located in proximity of the junction but do not face the T tubules. Two other such rows are present on the hidden side of the triad. The parajunctional feet interact with each other

Table 1. Comparison of parajunctional to junctional feet ratios and RyR3 to RyR1 ratios in a variety of muscles

	Toadfish swim muscle	Frog hind limb	Toadfish swim bladder	Mouse diaphragm, day 7	Mouse EDL, day 10
Ratio	1.6 ± 0.6	1.1 ± 0.7	0.0 ± 0.0	0.4 ± 0.4	0.2 ± 0.3
Parajunctional/junctional feet	n = 163	n = 536	n = 156	n = 385	n = 808
Ratio RyR3/RyR1	≥1*	~1†	0‡	Low§	Very low¶

*Refs. 9, 14, 21, and 39.
†Refs. 12 and 23.
‡Refs. 9 and 14.
§Refs. 10, 13, 15, 16, 25, and 40.
¶Refs. 10, 13, 15, 16, and 25.

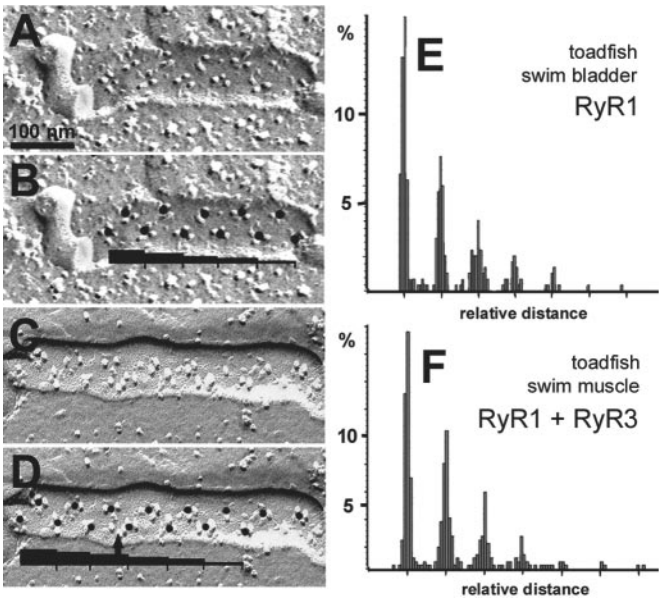

Fig. 5. Freeze–fractures showing cytoplasmic leaflets of T tubules. (*A*, *B*) Toadfish swim bladder (no RyR3); (*C*, *D*) toadfish white swim muscle (≈50% RyR3). DHPR tetrads are arranged in two parallel rows, and their centers are marked by a dot in *B* and *D*. (*E*, *F*) Frequency histograms of intertetrad spacings, measured as described in the text, showing a periodic positioning of tetrads. Intertetrad distances are twice the distance between feet independently of the presence or absence of RyR3.

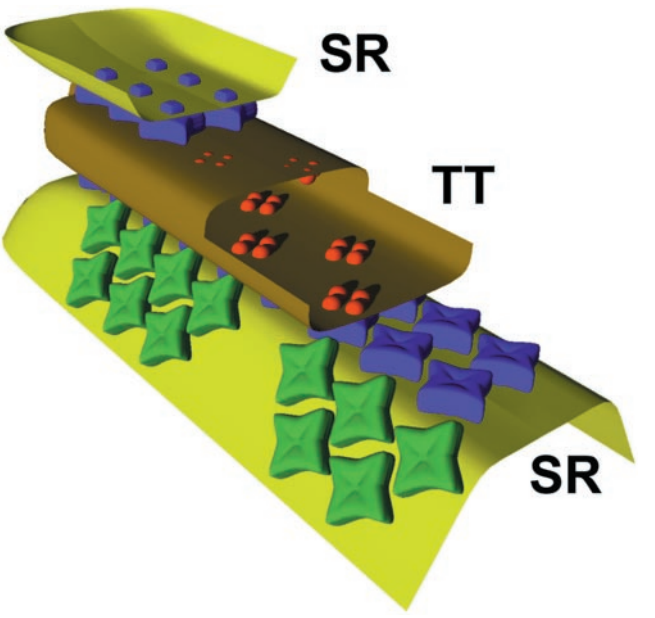

Fig. 6. Triad model for a muscle with two RyR isoforms. A double row of orthogonally placed junctional feet (dark profiles) occupies the gap between T tubule (TT) and SR sacs (SR). Light-colored parajunctional feet are located in the adjacent SR membrane, which faces toward the myofibrils. They are separated by a small zigzag strip from the junctional feet and are arranged in a zigzag pattern. Note that the spacing between the two rows of parajunctional feet is smaller than the spacing between the two junctional rows, explaining why the junctional feet in Fig. 1 *A–D* are more frequently seen as discrete profiles than the parajunctional feet.

quite differently from the junctional feet to fit into the observed lattices in the two locations. The parajunctional feet lattice has the same longitudinal spacing, but a shorter distance between the rows than the junctional lattice. The parajunctional feet are more closely fitted together, leaving less empty space than the junctional feet, which explains why the two rows of junctional feet are seen as clearly separate in the thin-section views of Fig. 1 *A–D*, whereas the two rows of parajunctional feet are not distinctly separated.

The four rows of parajunctional feet (two on either side) are discontinuous and/or shorter than the rows of junction feet for each triad. This detail fits the observation that in many images of triads, such as those shown in Fig. 1 *B* and *C*, parajunctional densities are not present at all four possible locations. If the parajunctional rows of feet were of the same length as the junctional rows, the parajunctional to junctional feet ratio would be 2:1, whereas the measured ratios are smaller.

The sketch applies to muscles with a high RyR3/RyR1 ratio. Triads in other skeletal muscles, e.g., from the mouse, have a single quite incomplete row of parajunctional feet on either side.

Discussion

Our data show that the presence and frequency of parajunctional SR feet in the triads of a variety of muscles correlate strictly to the presence and relative abundance of RyR3 in the same muscles, indicating that RyR3 are located somewhere within the six rows of junctional and parajunctional feet. It is conceivable that both types of feet might be mixed in both locations, because they might simply not fit into the limited junctional space. However, several lines of morphological evidence lead us to believe that RyR3 are instead segregated away from RyR1, so that RyR1 occupy the junctional domains of the SR and RyR3 are restricted to the parajunctional regions. All of the darker profiles in Fig. 6 would then represent RyR1 and the lighter profiles RyR3. A minor intrusion of RyR3 in to the junctional region, and the presence if some RyR1 in the parajunctional region can of course not be totally excluded.

The reasoning behind the conclusion that the two isoforms are segregated from each other and that parajunctional feet are not an equal mixture of RyR1 and RyR3 is as follows. If RyR3 were randomly and equally mixed with RyR1 in both junctional and parajunctional regions, the disposition of feet in the two areas would be the same. Instead, we find an abrupt transition between the tetragonal ladder-like arrangement of feet in the junctional region and the zigzag pattern of feet in the parajunctional areas. In Fig. 6, we illustrate a possible disposition of feet that would give rise to the two observed lattices and to the transition between them. To produce the two arrangements, the junctional and parajunctional feet interact quite differently with each other within each area, and a distinct break separates the two sets. This separate and distinct arrangement of junctional and parajunctional feet, probably because of different isoform composition, is in direct contrast to the structure of calcium release units in scorpions and spiders, which presumably have a single RyR isoform, as do other invertebrates (28, 29). The junctional and parajunctional feet in this case form part of a single continuous and congruent array (30, 31), showing that self-assembly properties of RyRs, and not their position in the junction, dictate the array lattice parameters.

A second, indirect piece of evidence for the separate position of RyR3 is related to the disposition of DHPR tetrads. In the RyR1-only muscle of the toadfish swim bladder, as well as in the swim muscle from the same species, which contains approximately 50% of RyR3, tetrads are located in exact superimposition of alternate feet. If RyR3 were randomly mixed with RyR1 in the junctional region of swim muscle, some flaws in this regular arrangement would occur, because RyR3 do not support tetrad formation (17). The observed regularly alternate disposition of tetrads would require a perfectly alternate checker-

board arrangement of RyR1 and RyR3 in the junctional region. If enough RyR3 participate in that disposition, both isoforms would also have to be largely present in the parajunctional regions, to maintain the observed RyR3/RyR1 ratio. However, we have already noted above that a homogenous composition of the six rows of feet is not consistent with their different structure. The above argument, of course, cannot exclude some intrusion of RyR3 in alternate position between feet of the junctional region. However, this intrusion would have to be limited, thus leaving most of RyR3 in the parajunctional region.

The fairly precise quantitative correspondence of RyR3/RyR1 ratio reported in the literature and our data, coupled with the arguments above showing that the two isoforms cannot be equally mixed in the junctional and parajunctional regions, also argues for a more or less complete separation of the two.

Given our hypothesis of a junctional location of RyR1 and a parajunctional location of RyR3, an obvious question is what mechanism segregates the two isoforms. One possibility is that the two are simply not sufficiently compatible to allow mixing in a common arrangement. The disposition of RyR1 in the junctional gap requires precise intimate contacts between the molecules (32). The small amount of extra mass of RyR1 relative to RyR3 (33) might very well impede the intimate contacts between the two molecules that is necessary for the formation of a regular lattice with mixed content. Such an exclusion would explain the apparent discrepancy between a possible segregation of RyR3 from the *in vivo* junctions and the junctional location of RyR3 expressed in dyspedic cells (17). In the dyspedic cells RyR1 was totally absent and lack of the suggested RyR1 "repelling" effect would enable RyR3 to enter the junctional sites.

Regardless of whether RyR3 and RyR1 are totally segregated, as we have suggested, or partly mixed in the junction, the activation of RyR3 is necessarily indirect, because RyR3 is not capable of being activated by skeletal DHPR (20). Thus, it is expected that RyR3 activation is a secondary event in e-c coupling, and that it follows the primary activation of RyR1 by DHPR (34), resulting in its amplification. Parajunctional feet do not seem to be in a close contact with junctional feet, which would exclude functional pairing between parajunctional RyR3 and junctional RyR1, of the type suggested for RyR1 by Marx *et al.* (35). The most likely possibility is that RyR3 are activated by the wave of Ca^{2+} resulting from opening of RyR1 (7, 34, 36, 37). Indeed a "dual control" of Ca release and an effect of RyR3 presence on the size of calcium sparks have been demonstrated (38, 39). It should be noted that in RyR1-only muscles, half of the RyR1 may also be activated indirectly (9, 32).

What then is the function of RyR3, or which beneficial effects could have resulted from the elimination of this isoform from certain muscles during evolution (9)? In fish (9, 14), there is a correlation between absence of RyR3 and rapidity of the contraction–relaxation cycle, consistent with the requirement for a rapid tightly controlled release of Ca^{2+} in fast muscles. However, it turns out that RyR3 content is not always well correlated to fiber type (13), and extraocular muscles of fish and bird totally lack RyR3 but have a varied fiber type composition (9).

This work was supported by National Institutes of Health Grant PO 144650.

1. Schneider, M. F. & Chandler, W. K. (1973) *Nature (London)* **242,** 244–246.
2. Rios, E. & Brum, G. (1987) *Nature (London)* **325,** 717–720.
3. Tanabe, T., Beam, K. G., Adams, B. A., Niidome, T. & Numa, S. (1990) *Nature (London)* **346,** 567–569.
4. Franzini-Armstrong, C. & Nunzi, G. (1983) *J. Muscle Res. Cell Motil.* **4,** 233–252.
5. Block, B. A., Imagwa, T., Campbell, K. & Franzini-Armstrong, C. (1988) *J. Cell Biol.* **107,** 2587–2600.
6. Franzini-Armstrong, C. & Protasi, F. (1997) *Physiol. Rev.* **77,** 699–729.
7. Sutko, J. L. & Airey, J. A. (1996) *Physiol. Rev.* **76,** 1027–1071.
8. Ogawa, Y., Kurebayashi, N. & Murayama, T. (1999) *Adv. Biophys.* **36,** 24–64.
9. O'Brien, J. O., Meissner, G. & Block, B. A. (1993) *Biophys. J.* **65,** 2418–2427.
10. Flucher, B., Conti,A., Takeshima, H. & Sorrentino, V. (1999) *J. Cell Biol.* **146,** 621–629.
11. Airey, J. A., Beck, C. F., Murakami, K., Tanksley, S. J., Deerinck, T. J., Ellisman, M. H. & Sutko, J. L (1990) *J. Biol. Chem.* **265,** 14187–14194.
12. Lai, F. A., Liu, Q.-Y., Xu, L., El-Hashem, A., Kramarcy, N. R., Sealock, R. & Meissner, G. (1992) *Am. J. Physiol.* **263,** C365–C372.
13. Conti, A., Garza, L. & Sorrentino, V. (1996) *Biochem. J.* **316,** 19–23.
14. Block, B. A., Brien, J. & Franck, J. (1996) in *Organellar Ion Channels and Transporters*, eds. Clapham, D. E & Ehrlich, B. E. (Rockefeller Univ. Press, New York), pp. 47–65.
15. Murayama, T. & Ogawa, Y. (1997) *J. Biol. Chem.* **272,** 24030–24037.
16. Bertocchini, F., Ovitt, C. E., Conti, A., Barone, V., Schoeler, H. R., Bottinielli, R., Reggiani, C. & Sorrentino, V. (1997) *EMBO J.* **16,** 6956–6963.
17. Protasi, F., Takekura, H., Wang,Y., Chen, S. R. W., Meissner, G., Allen, P. D. & Franzini-Armstrong, C. (2000) *Biophys. J.* **79,** 2494–2508.
18. Takeshima, H., Lino., M., Takekura, H., Nishi, M., Kuno, J., Minowa, O., Takano H. & Noda, T. (1994) *Nature (London)* **369,** 556–559.
19. Percival, A. L., Williams, A. J., Kenyon, J. L., Grinsell, M. M., Airey, J. A. & Sutko J. L. (1994) *Biophys. J.* **67,** 1834–1850.
20. Fessenden, J. D., Wang, Y., Moore, R. A., Chen, S. R., Allen, P. D. & Pessah, I. N. (2000) *Biophys. J.* **79,** 2509–2525.
21. Takeshima, H., Ikemoto, T., Nishi, M., Nishijama, N., Shimuta, M., Sugitani, Y., Kuno, J., Saito, I., Saito, H., Endo, M., Lino, M. & Noda, T. (1996) *J. Biol. Chem.* **271,** 19649–19652.
22. Murayama, T. & Ogawa, Y. (1994) *J. Biochem.* **116,** 1117–1122.
23. Olivares, E. B., Tanksley, S. J., Airey, J. A., Beck, C. F., Ouyang, Y., Deerinck, T. J., Ellisman, M. H. & Sutko, J. L. (1991) *Biophys. J.* **59,** 1153–1163.
24. Jeyakumar, L. H., Copello, J. A., O'Malley, A. M., Wu, G.-M., Grassucci, R., Wagenknecht, T. & Fleischer, S. (1998) *J. Biol. Chem.* **273,** 16011–16020.
25. Tarroni, P., Rossi, D., Conti, A. & Sorrentino, V. (1997) *J. Biol. Chem.* **32,** 19808–19813.
26. Stern, M. D., Pizarro, G. & Rios, E. (1997) *J. Gen. Physiol.* **110,** 415–440.
27. Ferguson, D. G., Schwartz, H. W. & Franzini-Armstrong, C. (1984) *J. Cell. Biol.* **99,** 1735–1742.
28. Xiong, H., Feng, X., Gao, L., Xu, L., Pasek, D. A., Seok, J. H. & Meissner, G. (1998) *Biochem. J.* **37,** 4804–4814.
29. Takeshima, H., Nishi, M., Iwabe, N., Miyata, T., Hosoya, T., Masai, I. & Hotta, Y. (1994) *FEBS Lett.* **337,** 81–88.
30. Gilai, A. & Parnas, I. (1972) *J. Cell Biol.* **52,** 626–638.
31. Loesser, K. E., Castellani, L. & Franzini-Armstrong, C. (1992) *J. Muscle Res. Cell Motil.* **13,** 161–173.
32. Yin, C. C. & Lai, F. A. (2000) *Nat. Cell Biol.* **2,** 669–671.
33. Sharma, M. R., Jeyakumar, L. H., Fleischer, S. & Wagenknecht, T. (2000) *J. Biol. Chem.* **275,** 9485–9491.
34. Rios, E. & Pizarro, G. (1988) *News Physiol. Sci.* **3,** 223–227.
35. Marx, S. O., Ondrias, K. & Marks, A. R. (1998) *Science* **281,** 818–821.
36. Percival, A. L., Williams, A. J., Kempon, J. L., Grinsell, M. M., Airey, J. A. & Sutko, J. L. (1994) *Biophys. J.* **67,** 1834–1850.
37. O'Brien, J., Valdivia, H. H. & Block, B. A. (1995) *Biophys. J.* **68,** 471–482.
38. Klein, M. G., Cheng, H., Santana, L. F., Jiang, Y. H., Lederer, W. J. & Schneider, M. F. (1996) *Nature (London)* **379,** 455–458.
39. Conklin, M. W., Barone,V., Sorrentino, V. & Coronado, R. (1999) *Biophys. J.* **77,** 1394–1403.
40. Giannini, G., Conti, A., Mammarella, S., Scrobogna, M. & Sorrentino, V. (1995) *J. Cell Biol.* **128,** 893–904.